How to cite this article: Tao H, Chen G, Lian C, Liu H, Coppens M-O. Multiscale modeling of ion transport in porous electrodes. *AIChE J.* 2022;e17571. doi:10.1002/aic.17571

Multiscale modelling of ion transport in porous electrodes

Haolan Tao[1#], Gong Chen[3#], Cheng Lian[1,2*], Honglai Liu[1,2], and Marc-Olivier Coppens[4*]

[1] State Key Laboratory of Chemical Engineering and Shanghai Engineering Research Center of Hierarchical Nanomaterials, School of Chemical Engineering, East China University of Science and Technology, Shanghai, 200237, China

[2] School of Chemistry and Molecular Engineering, East China University of Science and Technology, Shanghai, 200237, China

[3] Technology and Process Development (TPD), WuXi Biologics, 288 Fute Zhong Road, Waigaoqiao Free Trade Zone, Shanghai 200131, China

[4] Centre for Nature Inspired Engineering, and Department of Chemical Engineering, University College London, Torrington Place, London WC1E 7JE, UK

[*]Correspondence concerning this article should be addressed to C. Lian at liancheng@ecust.edu.cn, and M.-O. Coppens at m.coppens@ucl.ac.uk.

[#]These authors contributed equally to this work.

Abstract

Ion transport through nanoporous materials is of fundamental importance for the design and development of filtration membranes, electrocatalysts, and electrochemical devices. Recent experiments have shown that ion transport across porous materials is substantially different from that in individual pores. Here, we report a new theoretical framework for ion transport in porous materials by combining molecular dynamics (MD) simulations at the nanopore level with the effective medium approximation (EMA) to include pore network properties. The ion transport is enhanced with the combination of strong confinement and dominating surface properties at the nanoscale. We find that the overlap of electric double layers (EDLs) and the ion-water interaction have significant effects on the ionic distribution, flux, and conductance of electrolytes. We further evaluate the gap between individual nanopores and complex pore networks, focusing on the pore size distribution and pore connectivity. Our work highlights unique mechanisms of ion transport in porous materials important for practical applications.

Keywords: Ion transport, molecular dynamics simulations, effective medium approximation, pore-size distribution, pore connectivity

1. Introduction

Understanding ion transport confined in nanopores plays a crucial role in guiding the analysis and design of promising energy storage and conversion applications, such as blue energy harvesting,[1, 2] supercapacitors,[3, 4] fuel cells and batteries.[5] Pore confinement and surface charge effects make ion transport in nanopores complicated and drastically different from that in bulk systems.[6-9] In recent years, although some experimental techniques have been applied to study the dynamics of confined ionic fluids, such as the electrochemical quartz crystal microbalance (EQCM) and NMR spectroscopy,[10-12] investigating ion transport confined in a nanostructured electrode precisely remains challenging, and will require further developments of advanced characterization methods. Therefore, simulation methods, including continuum and molecular modelling, are attractive as alternative approaches to study ion transport in porous electrode. However, the study of electrokinetic transport in nanopores based on continuum models ignores the discrete nature of ionic species in the electrolyte.[13, 14] Although such approaches work well at low salt concentrations and small surface charge densities, the mean-field method has some problems for highly correlated systems.[15] Given the limitations of continuum modelling, some modifications of the conventional ion transport models have been developed, including ion excluded-volume effect,[16, 17] electrostatic correlations,[18] electric double layer (EDL) overlap,[19] ion-wall interactions,[20, 21] and surface reactions.[22] Generally, all of these modifications need to be considered to reproduce experimental data for ionic transport in nanochannels,[14] which makes the theoretical framework rather complex, and, thus, a unified theoretical framework that captures the picture in its entirety is still missing.

Compared with the continuum theoretical framework, molecular dynamics (MD) simulations are a more effective method to study the distribution of ions and water molecules with an emphasis on the role of ion hydration and ion-ion electrostatic interactions on the ion distribution inside a pore. Feng *et al.*[23] have studied the distribution of K^+ ions in charged slit

pores with widths ranging from 9.36 to 14.7 Å using MD simulations. They showed that a well-hydrated single layer of K^+ ions was formed in the centre of negatively charged nanochannels, which differs qualitatively from the prediction by the classical EDL theories and is caused primarily by the ion hydration effects. Qiu *et al.*[24] have explained the origin and properties of EDL capacitance in short graphene nanochannels with widths below 2 nm using MD simulations. The nonmonotonic dependence of capacitance on the channel width was attributed to the width-dependent radial location of counter-ions in the nanochannels and the restricted number of co-ions. Su *et al.*[25] used MD simulations to study the coupling between transport of water and ions through a carbon nanotube under electric fields. They studied the role of ionic conditions, including salt species and concentration. They found that the coupling of water and anions is stronger than between water and cations, and, thus, anions play a dominant role in determining the water transport.

Although great progress has been made in understanding ion transport in individual nanochannels in recent years, less attention has been paid to ion transport through nanoporous materials with different pore connectivity and pore size distributions.[26, 27] A single-pore model cannot sufficiently reflect the heterogeneity of pore networks, like those in carbon-based membranes and porous electrodes.[28] Compared to understanding the electrokinetic transport in individual nanochannels, investigating the transport properties of ions confined in nanoporous materials as a whole is more difficult, because of the stochastic nature and distribution of multiscale complex and imperfect pore structures within the bulk material.[29]

In this work, we report a multiscale theoretical framework to describe ion transport through porous carbon electrodes by combining MD simulations and the effective medium approximation (EMA). The transport properties of individual slit pores are computed using MD simulations, considering the role of ion hydration and long-range ion-ion electrostatic interactions on the ion distribution inside a nanochannel. For comparison, the Poisson-Nernst-

Planck and Navier–Stokes (PNP-NS) equations were also used to study ion transport through the same individual nanochannels, but this leads to large deviations from MD simulations, demonstrating the limitations of such continuum models. The adoption of EMA allows us to bridge the gap between single pores and porous medium that is typical for porous carbons and membranes. The results from the MD-EMA predictions reveal the important influence of the pore size distribution and network connectivity on the ionic conductance in nanoporous materials.

2. Molecular model and methods

2.1 Model setup

This study focuses on ion transport through nanoporous carbon electrodes, in contact with a bulk electrolyte. Connecting the ionic transport properties in the porous materials to their pore networks directly remains challenging, as it requires a large amount of micro-structural data, which is difficult to implement. Here, a multiscale model has been developed to understand the ion transport in porous materials by combining molecular dynamics (MD) simulations with the effective medium approximation (EMA). Transport properties in individual slit pores are computed using MD simulations. MD results are compared with those computed using a continuum model, based on the PNP-NS equations, to study ion transport through an individual nanochannel with the same pore size and simulation conditions. The EMA is used to construct an "effective" porous medium that has the same pore size distribution and pore network parameters of realistic porous materials. Combined with the MD simulation results, this allows us to obtain effective properties of the original porous material, incorporating the transport properties of individual pores.

2.2 Molecular dynamics simulations

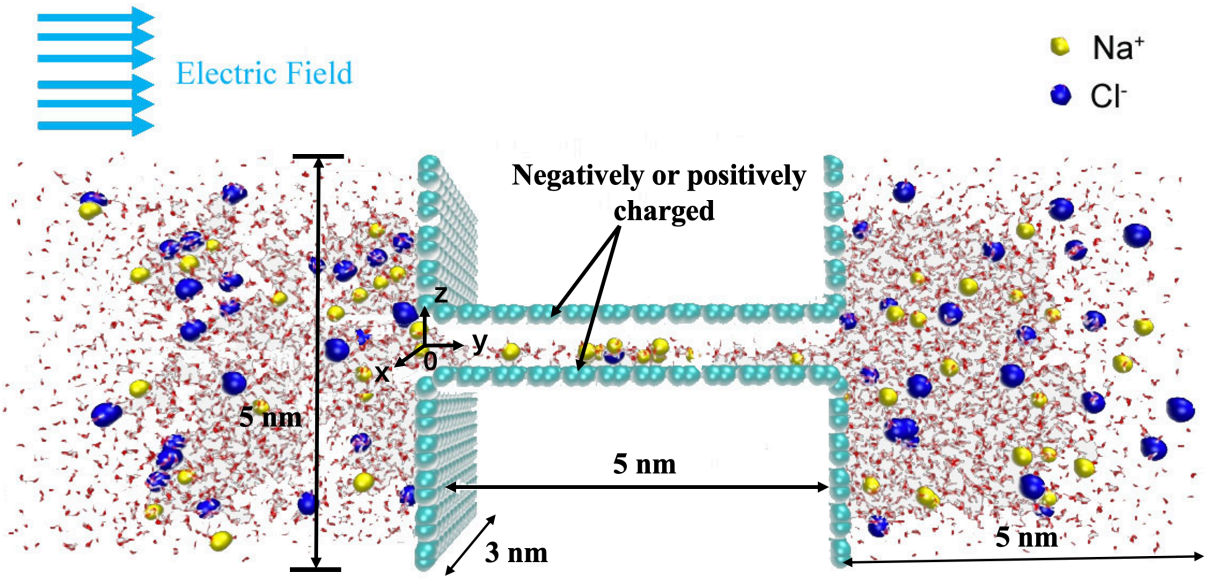

Figure 1. Schematic of ion transport in a nanopore. A slit pore with a length of 5 nm and width (pore size) varying from 0.75 nm to 2.5 nm is contained between two graphene sheets (3×5 nm^2), and is placed in a periodic water box with water molecules and some Na^+ and Cl^- ions with an ionic concentration of 2 M. A static electric field of $E = 0.1$ V/nm along the y-direction is applied to the whole box.

Figure 1 presents the configuration on which the molecular dynamics (MD) simulations are based, to describe the coupled transport of ions and water through an individual, slit-shaped nanopore in an electric field, parallel to the pore. The 5 nm long slit is contained between two graphite sheets (3×5 nm^2). Its pore size, corresponding to the slit width, is varied. All MD simulations are implemented at constant volume and temperature (Nose-Hoover coupling) in the GROMACS 4.5 simulation package.[30] The SPC/E water model is used to model water molecules.[31, 32] The CHARMM36-jun2015 force field is used to describe the carbon and ion interactions.[33, 34] A similar force field has been used in many reported studies to describe the nanofluidic system and ion transport.[35] Specifically, in this system, the graphene atoms are charged and their positions are fixed as part of the pore walls, thus only the nonbonded interaction between the graphene atoms and H_2O, Na^+, Cl^- should be considered. In **Table 1**,

we list the L-J parameters and the partial charges used in this study. The particle-mesh Ewald method is used to treat the long-range electrostatic interactions among ions, water molecules, and surface charges.[36] The cutoff used for the short-range interaction is 1.2 nm. A static electric field of E = 0.1 V/nm along the y-direction is applied to the whole box, driving ions and water molecules through the channel. Periodic boundary conditions are applied to the x, y and z directions. The solution system is maintained at 300 K by a modified Berendsen thermostat.[31] A time step of 2 fs is used to integrate the equations of motion by a leapfrog algorithm, and the data are saved every 0.2 ps. The first run lasting 100 ns is used to equilibrate the system; another 100 ns long run follows to gather the statistical quantities.

	site	σ/nm	ε/kJ mol^{-1}	q/e
Ions	Na+	0.251	0.1962	1.000
	Cl-	0.404	0.6275	-1.000
Water	O_w	0.317	0.6502	-0.8476
	H_w	0.000	0.0000	0.4238
Pore	C (charged)	0.355	0.3598	q_c/e
Wall	C (neutral)	0.355	0.3598	0.000

Table 1. The Lennard-Jones parameters and partial charges for ions and (SPC/E) water molecules[31, 32] in the slit pore, and the carbon atoms of its walls.

To consider the difference between a positively charged and a negatively charged slit pore surface, the surface charge density is, respectively, set as σ_s = +0.1 C/m^2 and σ_s = -0.1 C/m^2. Specifically, the charge of each C atom of the slit pore is calculated using the equation:

$$q_C = \frac{\sigma_s \times A}{N}, \tag{1}$$

where A represents the charged area, and N is the number of charged carbon atoms. To study the effect of channel confinement, the slit width (pore size) is varied from 0.75 nm to 2.5 nm. For each pore size, the density profile of ions and water is calculated in the z- and y-direction, as well as the ion fluxes through the pores. An equivalent electrical circuit can be calculated from the mean of the ion fluxes, $\vec{J}_i(d)$, through a slit of pore size, d:

$$I = A\sum_i z_i e\vec{J}_i(d), \tag{2}$$

where A is the cross-sectional area of the slit. Ion transport through a nanopore is typically measured in terms of the conductance, $G = I/V$, *i.e.*, the ionic current, I, divided by the voltage drop, V. Here, a local drop of the voltage through the nanochannel is 0.1 V/nm × 5 nm = 0.5 V. In this work, the roles of ion type and concentration are not considered. Attention is focused on 2 M NaCl in water.

2.3 Continuum modeling

The first equation to consider is the Nernst-Planck Equation, which is a conservation of mass equation that describes the influence of an ionic concentration gradient and that of an electric field on the flux of ions. The general conservation of mass equation is expressed as:

$$\frac{\partial c_i}{\partial t} + \nabla \cdot \vec{J}_i = 0, \tag{3}$$

where c_i is the molar concentration of the ith ion species. In what follows, a NaCl solution is considered, with $i = 1$ for Na^+ and $i = 2$ for Cl^-. Furthermore, the flux $\vec{J}_i$ of ion species i within the solution is given by the following constitutive equation:

$$\vec{J}_i = -D_i(\nabla c_i + \frac{z_i F c_i}{RT}\nabla\phi) + c_i\vec{u}, \tag{4}$$

where the first term is the flux due to diffusion and the second term is the flux due to electro-migration in the electric field; in addition, $\vec{u}$ is the mass-averaged velocity of the solvent; z_i is the ith ion valence, D_i is the ion diffusivity in aqueous solution, T is the absolute temperature, and F and R are the Faraday constant and the ideal gas constant, respectively. The electrostatic potential profile ϕ satisfies the Poisson equation:

$$\rho_v = \nabla \cdot (-\varepsilon\nabla\phi), \tag{5}$$

where ρ_v is the free space charge density, and ε is the permittivity of the solution. Using a mean field approximation, another equation for the free space charge density is posited, which is

defined in terms of the mean (volume averaged) ion concentrations:

$$\rho_{\mathrm{v}} = F\sum_{i} \mathrm{z}_i c_i. \tag{6}$$

For an incompressible laminar flow, the fluid movement is governed by the continuity and the Navier-Stokes (NS) equations:

$$\nabla \cdot \vec{\mathrm{u}} = 0, \tag{7}$$

$$\rho \frac{\partial \vec{\mathrm{u}}}{\partial t} = -\nabla P + \eta \nabla^2 \vec{\mathrm{u}} + F_e, \tag{8}$$

where ρ is the fluid density, P is the pressure, and η is the dynamic fluid viscosity. F_e can be any kind of external body force, but, here, it is the electrical driving force:

$$F_e = -\rho_{\mathrm{v}} \nabla \phi. \tag{9}$$

The above governing equations can be solved for specified boundary conditions, which are the same as for the MD simulations, discussed in the previous section. The detailed setup for PNP-NS calculations is shown in the Supporting Information (SI).

2.4 Effective medium approximation

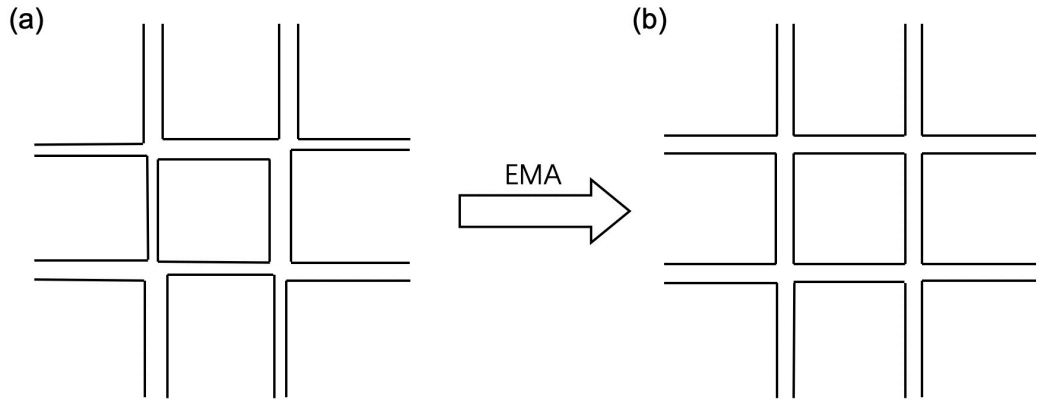

Figure 2. In EMA, the conductance of a discrete network of pores with different pore sizes **(a)** is calculated as an 'effective' conductance of a network of the same topology, with pores that all have the same size **(b)**.

Based on the results of MD simulations in individual nanopores, the effective medium approximation (EMA) is used to calculate the overall, effective ion transport in porous materials, consisting of a network of nanopores. The basic concept of discrete (as opposed to continuous) EMA, as introduced by Kirkpatrick,[37] considers an equivalent electrical resistor network. Applied to pore networks, as schematically shown in **Figure 2**, this method consistently replaces the pores in a heterogeneous network of a disordered porous material by a hypothetical, homogeneous network of individual pores that all have the same conductance, whilst preserving the pore network connectivity; the effective transport properties of this uniform network can then be calculated easily. According to EMA, the effective conductance, G_{eff}, can be estimated from:

$$\sum_{d=d_{\min}}^{d=d_{\max}} P(d)\frac{G_{eff}-G_d}{\left(\frac{Z}{2}-1\right)G_{eff}+G_d}=0, \tag{10}$$

where Z is the average network connectivity, *i.e.*, the average number of pores connected to each node in the pore network; G_{d} is the conductance of a pore with pore size d; $d_{\min}$ and $d_{\max}$ are the minimum and maximum pore sizes; $P(d)$ is the probability distribution of the pore size in the range $[d_{\min}, d_{\max}]$.

The high accuracy of the EMA method to investigate transport properties in pore networks far enough from the percolation threshold has been confirmed by Burganos and Sotirchos through the comparison between the EMA method and "exact" Monte-Carlo simulations for various pore networks.[38] A recent review has further discussed the validation of the EMA method, which indicates that the EMA method can reproduce the results of detailed computer simulations very well.[39] Thus, it is an effective approach to test the effects of connectivity and pore size distribution of the original nanoporous materials.

3. Results and Discussion

3.1 Distribution of ions from MD simulations

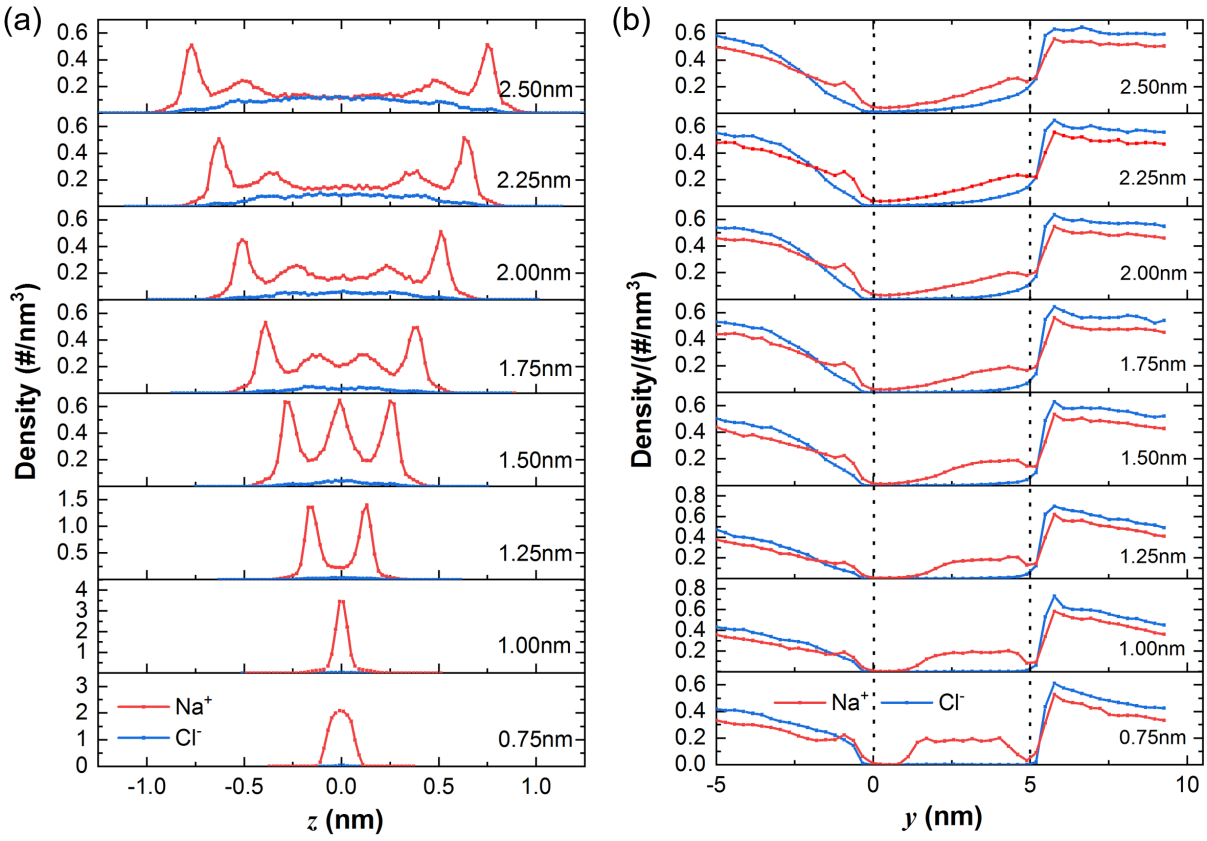

Figure 3. Ion distributions from MD simulations along **(a)** *z*-axis and **(b)** *y*-axis in negatively charged nanochannels with a width increasing from 0.75 nm to 2.50 nm. The surface charge density is −0.1 C/m^2. The dotted vertical lines in (b) indicate the nanochannel's boundaries.

The MD-simulated distributions of counter-ions (Na^+) and co-ions (Cl^-) perpendicular to the surfaces of the negatively charged nanochannels with different widths are plotted in **Figure 3a**. The distribution of Na^+ counter-ions displays multiple peaks when the nanochannel is wider than 1 nm, which is similar to the result in an ionic-liquid electrolyte.[40] Notable changes occur between 1 and 1.25 nm (from one to two peaks), 1.25 and 1.5 nm (from two to three peaks), and 1.5 and 1.75 nm (three to four peaks). As the pore size increases to more than 1.75 nm, near each of the carbon surfaces, two significant peaks appear, a large one and a small one,

which shows that Na^+ ions mainly accumulate in two layers located 0.5 and 0.75 nm away from each surface. When the pore size is 2.5 nm, a neutral region in the center of slit pore appears, which has no contribution to the net flux. However, as the width of the channel decreases, the number of Na^+ ion aggregation peaks shrinks, whereas the number of Na^+ in each individual layer increases substantially, which may be attributed to the overlap of the electrical double layer (EDL) caused by the increased constriction imposed by the nanochannel. As a result of the electrostatic repulsion generated by the negative surface charges, Cl^- ions mainly appear in the center of pores with sizes beyond 1.5 nm. As the channel shrinks, it becomes harder for Cl^- ions to enter the channels, becoming nearly impossible when the channel width drops to 1.25 nm. When the pore size dips below 1 nm, Cl^- ions are virtually excluded from the pore, which can only accommodate Na^+ ions that are mainly contained within a single accumulation layer, confined between both surfaces.

A different picture is painted by the cross-sectionally averaged ion distributions in the *y*-direction, parallel to the surfaces of the negatively charged nanochannels with different widths, shown in **Figure 3b**. Driven by the electric field, the Na^+ cations travel along the positive *y* direction (red line), while the Cl^- anions are transported along the negative *y* direction (blue line). Therefore, many Na^+ ions are blocked outside the inlet ($y = 0$) of these narrow nanochannels, and, in the nanochannel, the Na^+ ions mainly accumulate in the region near the outlet ($y = 5$ nm). Due to the periodic boundary conditions, the Cl^- ions enter the slit pores from the opposite direction as well. Furthermore, it can be observed that the number of Na^+ ions is much larger than that of Cl^- ions in the nanochannels, but with opposite behavior in the reservoirs, which is due to the negatively charged pore walls. When the pore size is smaller than 1 nm, almost no Cl^- ions enter the nanochannel, as noted in **Figure 3a**. As the slit pore widens, more Cl^- ions can enter the nanochannel, and further move in the negative *y* direction. For a pore size between 0.75 nm and 1.75 nm, the density of Na^+ ions in the middle of the

nanochannel (1.25 nm < y < 3.75 nm) decreases. When the slit pore is wider than 2 nm, the density profile of Na^+ ions in the whole system hardly changes. Similar layered distributions of counter-ions in the positively charged nanochannels are shown in **Figure S1a**, whereas a different change of the aggregation peaks of counter-ions occurs between 1 and 1.5 nm (from two to four peaks), which is probably due to the different ion sizes and interactions between ions and water molecules.

3.2 Distribution of water solvent molecules in charged nanopores

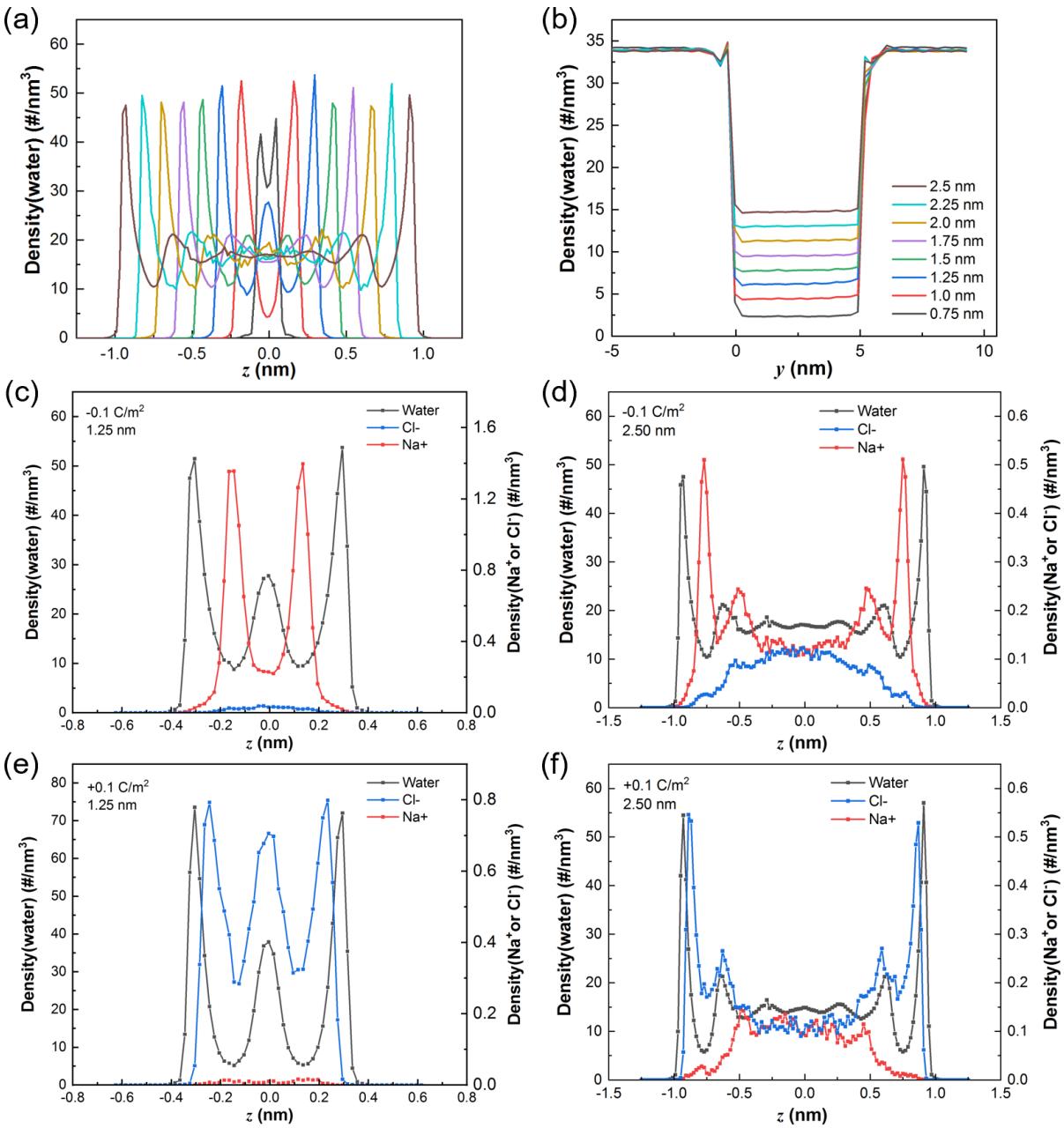

Figure 4. Density distributions of water molecules along **(a)** the *z*-axis and **(b)** the *y*-axis in the negatively charged nanochannels, with the width varying from 0.75 nm to 2.50 nm. The surface charge is -0.1 C/m^2 in every simulation. Distributions of ions and water molecules in slit nanopores with a surface charge density of -0.1 C/m^2 when the widths of the slits are **(c)** 1.25 nm and **(d)** 2.50 nm. Distributions of ions and water molecules in slit nanopores with a surface density of +0.1 C/m^2 when the widths of the slits are **(e)** 1.25 nm and **(f)** 2.50 nm.

The water molecule distributions in a cross-section of the nanochannels with different pore sizes are shown in **Figure 4a**; these reveal distinctly layered water distributions. The water distribution inside the nanochannels changes as the width increases: two aggregation peaks can be identified when $d < 1.25$ nm, while four and even more layers of water molecules are shown in the nanochannels with $d > 1.25$ nm. The two highest peaks are always located at approximately 0.4 nm away from each adjacent slit surface, as water molecules tend to stay near the graphene surfaces and form a contact water layer.[23] **Figure 4b** shows the cross-sectionally averaged density distributions of water molecules along the *y*-direction in negatively charged nanochannels with a width varying from 0.75 nm to 2.50 nm, which further indicates that the decrease in pore size negatively affects the accumulation of water molecules inside the nanochannels. However, the asymmetric distribution of ions along the *y*-direction (shown in **Figure 3b**) has little influence on the cross-sectionally averaged density of water molecules, because the number of cations and anions is much lower than that of water molecules (roughly two orders of magnitude lower).

The water molecule and ion distributions in 1.25 and 2.50 nm wide nanochannels along the *z*-direction are plotted together in **Figure 4c-f**, first for a surface charge density of -0.1 C/m^2 **(Figure 4c & d)**, then for +0.1 C/m^2 **(Figure 4e & f)**. From **Figure 4c-f** , it is found that the aggregation of water molecules plays an important role in the distribution of counter-ions, in

addition to the confinement imposed by the nanochannels.[24] From these figures, we can see a similarly shaped distribution of water molecules, Na^+ ions and Cl^- ions, while the peak positions vary. In a negatively charged channel, Na^+ ion peaks appear in the valleys of the water distributions, which is different to the Cl^- ion distributions in a positively charged channel. As shown in **Figure 4e-f**, the locations of Cl^- ion peaks follow those of the water distribution, which are closer to the surfaces of the channels. This is because water molecules are dominated by the charge and volume of oxygen atoms, and the coupling of water molecules to anions is stronger than that to cations.[25] It means that Cl^- ions show more affinity to water molecules, which can also explain the differences of ion distributions between negatively and positively charged nanochannels, as mentioned above.

3.3 Ionic distribution from continuum modelling

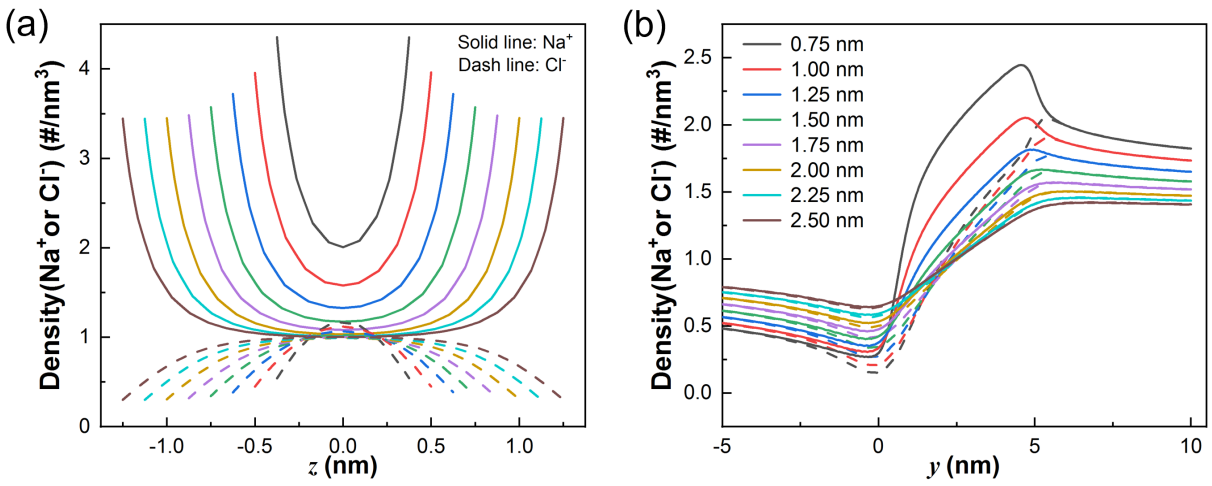

Figure 5. Ion distributions from continuum modelling along **(a)** z-axis (x = 0 nm, y = 2.5 nm) and **(b)** y-axis (x = 0 nm, z = 0 nm) in negatively charged nanochannels with a width increasing from 0.75 nm to 2.50 nm. The solid line is the density profile of Na^+, and the dashed line is the density profile of Cl^-. The surface charge density is −0.1 C/m^2. The bulk concentration of NaCl is 2 M.

The continuum model based on PNP-NS equations is used to study the ion transport through the same individual nanochannels, and the results are compared with those from MD

simulations. The counter-ions and co-ions distributions along the *z*-direction in the middle (y = 2.5 nm) of the negatively charged nanochannels with different widths are shown in **Figure 5a**. The density of counter-ions decreases sharply within ~0.5 nm from the surfaces of the nanochannels, while the density of co-ions increases gradually. As the pore size increases, the difference between the density of cations and anions along the *y*-direction in the centre of the nanochannels decreases, as shown in **Figure 5b**. A comparison between the MD simulations (**Figure 3**) and PNP-based continuum modelling (**Figure 5**) indicates that they predict the effect of pore size on the distribution of counter-ions differently. The MD simulations show a layered distribution of counter-ions along the *z*-direction near the surfaces of the nanochannel, in which these layers of counter-ion aggregation will overlap gradually as the channel shrinks, while the continuum model gives an upward, concave density profile of counter-ions along the *z*-direction, regardless of the widths of the nanochannels. In addition, we can see that the counter-ion densities near the surfaces of the nanochannels obtained from the continuum modelling are much higher than the results from MD simulations. These deviations can be attributed to the assumption of point species in the continuum model, which ignores the effects of excluded volumes and water molecules between ions. Using the same calculation approach, the ion distributions in a positively charged channel, shown in **Figure S2**, present qualitatively similar density profiles for the counter-ions and co-ions as in the case of a negatively charged channel. Thus, the PNP equations cannot describe the differences between Na^+ and Cl^- in the nanochannels.

The largest difference between the PNP-based continuum model and MD simulations is the distribution of water molecules, because the former method treats water as a continuum, while the latter one considers the water molecular profiles in nanoscale pores. Summarizing the last two sections, it is found that the water molecules play a non-negligible role in the structure of the EDL inside nano-confinements. As the PNP-based continuum model is not physically

reasonable, as opposed to MD simulations, the following discussions are all based on MD simulation results.

3.3 Pore size effect on ion transport

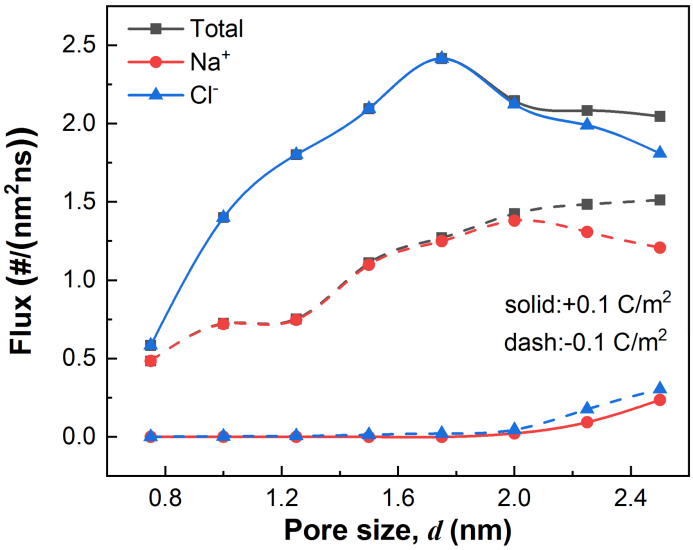

Figure 6. Cationic, anionic and total flux through slit-shaped nanochannels as a function of pore size, when the surface charge density is -0.1 C/m^2 or +0.1 C/m^2.

Figure 6 shows cross-sectionally averaged fluxes of counter-ions and co-ions along the *y*-direction through negatively and positively charged nanochannels, as a function of pore size, calculated from MD simulations. The flux of Cl^- in the positively charged nanochannels is always higher than the flux of Na^+ in the negatively charged nanochannels, which is attributed to the stronger coupling of water molecules and anions, as discussed earlier. Therefore, Cl^- counter-ions can pass through the channel more easily with an increase in pore size. When the pore size d < 2 nm, almost the entire contribution to the total flux comes from the flux of counter-ions, which shows a non-monotonic dependence on the pore size. For these total fluxes in different channels, a maximum is observed in a positively charged channel of 1.75 nm, while an unexpectedly low value is obtained in a negatively charged channel of 1.25 nm, which is attributed to the overlap of the EDLs. According to previous research for electroosmotic flow

in nanopores based on the classical density functional theory (CDFT) and the NS equation, due to the overlap of the EDLs, a pore-size dependent oscillatory behaviour of the conductivity was demonstrated, which can help us understand these special cases.[41] The difference between this CDFT-NS and MD simulation results are the amplitudes of the oscillations, where the former oscillates less, while the latter oscillates more, as only cations and anions in a continuum water solution are considered in the primitive model of the CDFT, while the discontinuous solvent (water) effects are taken into account in the MD simulations based on the all-atom models.[42] When the width of the slit pore increases to more than 2 nm, the confinement imposed by the channel becomes weak, and the surface potential is gradually shielded by the counter-ions, thus, co-ions could move through the slit pore. As shown in **Figure 4d-f,** the densities of cations and anions in the centre of the slit pore tend to be equal to the bulk concentration. Therefore, we can see that for both negatively and positively charged channels, when $d > 2$ nm, with the increase of pore size, the flux of counter-ions decreases while the flux of co-ions increases, but the total fluxes only slightly change, regardless of the increase in pore size.

3.4 Influence of pore size distribution and network connectivity on the ion transport

For the individual slit pore, the influences of pore size on the ion distribution and flux have been discussed above. Based on the results of ion fluxes obtained from MD simulations (**Figure 6)**, the conductance through the slit nanochannels with different pore sizes can be calculated using the equation (2), as shown in **Figure 7a**, which shows an increasing trend with the expansion of the slit pore. Corresponding to the higher ion flux, the electrolyte in the positively charged nanochannels has a higher conductance, which is attributed to the stronger coupling of water molecules and anions.

However, in practical porous electrodes, the pore structure is more complicated, and ion transport is also affected by the pore size distribution and pore network connectivity. Here, the

EMA is used to obtain effective properties of the porous material from the transport properties in individual slit pores.

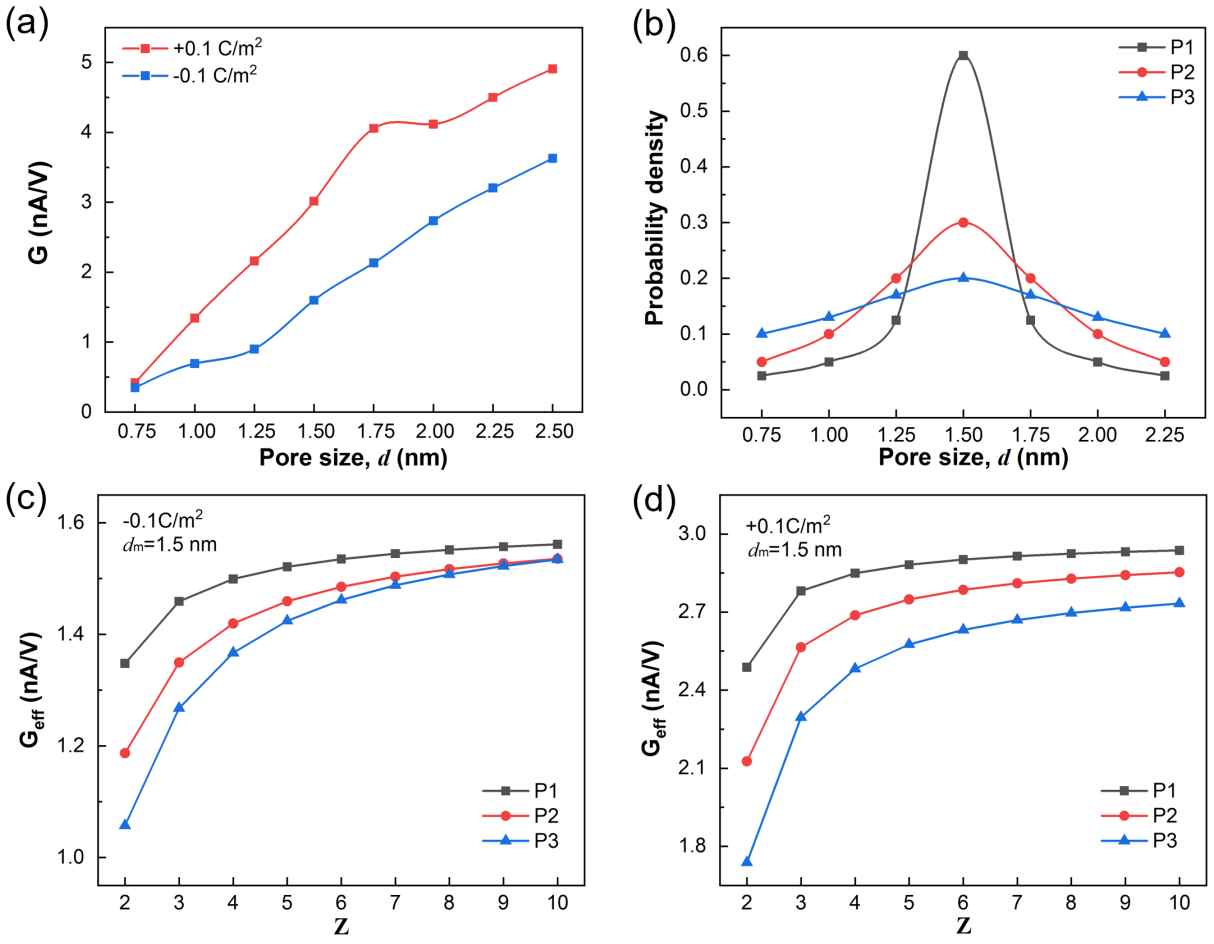

Figure 7. (a) Conductance, G, of 2 M NaCl in slit-shaped nanochannels with a width varying from 0.75 nm to 2.50 nm, and a surface charge density of +0.1 C/m^2 or -0.1 C/m^2. **(b)** Porous materials containing three different pore size distributions, P1, P2 and P3, are considered to study the difference between single pores and pore networks. The mean pore size, d_m, is 1.5 nm. Effective conductance, G_{eff}, of 2 M NaCl in porous carbon electrode models versus the pore connectivity parameter, Z, for different pore size distributions (P1, P2 and P3) when the surface charge density is **(c)** -0.1 C/m^2 and **(d)** +0.1 C/m^2.

To consider the effects of pore size distribution on ionic conductance, three pore size distributions with the same mean pore size, d_m = 1.5 nm, but different standard deviations are

considered. As shown in **Figure 7b**, P1 is the narrowest distribution among these three distributions, i.e., most pores have a size close to the mean pore size, d_m. P2 contains 30% of pores of size d_m, 20% of size $d_m \pm 0.25$ nm (each), 10% of size $d_m \pm 0.5$ nm (each), and 5% of size $d_m \pm 0.75$ nm (each). P3 has a nearly uniform distribution (10% ~20%), spread over seven pore sizes: d_m, $d_m \pm 0.25$ nm, $d_m \pm 0.5$ nm and $d_m \pm 0.75$ nm. These pores are all slit-shaped; the corresponding total pore volume and, thus, the porosity, are also the same. Based on the results in **Figure 7a** and equation (9), the effective conductance of these three pore networks, P1-P3, is computed by EMA as a function of network connectivity. The results are plotted in **Figure 7c-d**, which shows that P1>P2>P3 for the effective conductance, independent of pore network connectivity, suggesting that the connectivity effect is secondary to that of the pore size distribution. The pore network with the widest pore size distribution (P3) has a larger percentage of small pores, thus, has the lowest conductance, especially at low pore connectivity. This means that the pore size distribution must be accounted for. As the pore size distribution broadens, the conductance of a porous network is much smaller than that of an individual slit pore of the same mean size. To some extent, it may help us explain the giant gap between single-pore- and membrane-based nanofluidic osmotic power generators.[28] Previous research based on classical DFT and EMA has shown the influences of pore size distribution and network connectivity on the ionic transport within a large interval of d_m, which led to similar conclusions.[27]

When the pore network connectivity, Z, increases from 2 to 10, the effective conductance rises for any of these three pore networks with $d_m = 1.5$ nm. Simultaneously, the gap between the EMA conductance of the electrolyte in the three pore networks narrows, for both negatively and positively charged pores, as shown in **Figure 7c-d**. Furthermore, for the pore network with the wider pore size distribution (P3), the improvement of the effective conductivity is more obvious as the pore network connectivity increases. These results mean that the pore

connectivity of a porous material is an important parameter in determining its conductance, especially for a wide pore size distribution. As G_{eff} is a monotonically increasing function of Z, the two cases $Z = 2$ and $Z \to \infty$ provide bounds on G_{eff} that hold for all values of Z.[37] For the case of $Z = 2$, which represents a serially connected network, the effective conductance from the EMA agrees with the harmonic mean (as shown in **Figure S3)**, whereas, for $Z \to \infty$, the effective conductance can be calculated by the arithmetic mean, corresponding to parallel pores. Consequently, the EMA result lies in the closed interval defined by the harmonic and arithmetic means of the individual conductances.

4. Conclusions

A multiscale model for ion transport in porous materials was developed by combining molecular dynamics (MD) simulations at the nanopore level with the effective medium approximation (EMA) for the pore network. The transport behaviour predicted by a continuum model based on the PNP-NS equations deviates both qualitatively and quantitatively from that predicted by MD simulations, as the PNP-NS based approach does not account for excluded-volume, ion hydration and long-range ion-ion electrostatic interactions. This level of detail is included in MD simulations, which were consequently applied to study the transport properties of a 2M NaCl solution in individual slit pores, bounded by charged, graphite planes. Both steric and electrostatic confinement effects are induced by the slit nanopores; aggregation between water molecules affects ion transport through the pores as well. When the pore size dips below 1 nm, co-ions can hardly enter the pore. The aggregated water molecules show a layered distribution perpendicular to the surfaces when the slit pore size is more than 1 nm, which can affect the distribution of counter-ions, resulting in differences between the counter-ion distribution in positively and negatively charged pores. As the pore size increases, the flux of counter-ions has a maximum at about 1.8 nm. Subsequently, the effective conductance of three pore networks is computed by EMA to investigate the effects of pore-size distribution and pore

connectivity, while including the conductance in nanopores calculated by MD simulations. As expected, increases in mean pore size and pore connectivity enhance the effective conductance. In addition, ion transport is enhanced when the porous material has a narrow pore-size distribution. These results agree well with our previous research based on classical DFT and EMA. As an effective method to study the ion transport in porous materials, this multiscale model could be applied to investigate transport in porous materials relevant to electrochemical applications and separation processes.

AUTHOR INFORMATION

ORCID

Cheng Lian: orcid.org/0000-0002-9016-832X

Honglai Liu: orcid.org/0000-0002-5682-2295

Marc-Olivier Coppens: orcid.org/0000-0002-1810-2537

Notes

The authors declare no competing financial interest.

Acknowledgments

This work was also sponsored by the National Natural Science Foundation of China (No. 91834301, 22078088) and National Natural Science Foundation of China for Innovative Research Groups (No. 51621002). MOC gratefully acknowledges EPSRC for support via a “Frontier Engineering: Progression” award (EP/S03305X/1).

References

1. Siria, A.; Bocquet, M.-L.; Bocquet, L., New avenues for the large-scale harvesting of blue energy. *Nature Reviews Chemistry* **2017,** *1* (11), 0091.
2. Xiao, K.; Jiang, L.; Antonietti, M., Ion transport in nanofluidic devices for energy harvesting. *Joule* **2019,** *3* (10), 2364-2380.
3. Zhong, C.; Deng, Y.; Hu, W.; Qiao, J.; Zhang, J., A review of electrolyte materials and compositions for electrochemical supercapacitors. *Chemical Society Reviews* **2015,** *44* (21), 7484-7539.
4. Dou, Q.; Lei, S.; Wang, D.-W.; Zhang, Q.; Xiao, D.; Guo, H.; Wang, A.; Yang, H.; Li, Y.; Shi, S.; Yan, X., Safe and high-rate supercapacitors based on an "acetonitrile/water in salt" hybrid electrolyte. *Energy & Environmental Science* **2018,** *11* (11), 3212-3219.
5. Bazant, M. Z., Theory of chemical kinetics and charge transfer based on nonequilibrium thermodynamics. *Accounts of Chemical Research* **2013,** *46* (5), 1144-1160.
6. Comtet, J.; Nigues, A.; Kaiser, V.; Coasne, B.; Bocquet, L.; Siria, A., Nanoscale capillary freezing of ionic liquids confined between metallic interfaces and the role of electronic screening. *Nature Materials* **2017,** *16* (6), 634-639.
7. Gopinadhan, K.; Hu, S.; Esfandiar, A.; Lozada-Hidalgo, M.; Wang, F. C.; Yang, Q.; Tyurnina, A. V.; Keerthi, A.; Radha, B.; Geim, A. K., Complete steric exclusion of ions and proton transport through confined monolayer water. *Science* **2019,** *363* (6423), 145-147.
8. Mouterde, T.; Keerthi, A.; Poggioli, A. R.; Dar, S. A.; Siria, A.; Geim, A. K.; Bocquet, L.; Radha, B., Molecular streaming and its voltage control in angstrom-scale channels. *Nature* **2019,** *567* (7746), 87-90.
9. Sint, K.; Wang, B.; Kral, P., Selective ion passage through functionalized graphene nanopores. *Journal of the American Chemical Society* **2008,** *130* (49), 16448-16449.
10. Tsai, W. Y.; Taberna, P. L.; Simon, P., Electrochemical quartz crystal microbalance (EQCM) study of ion dynamics in nanoporous carbons. *Journal of the American Chemical Society* **2014,** *136* (24), 8722-8728.
11. Griffin, J. M.; Forse, A. C.; Tsai, W. Y.; Taberna, P. L.; Simon, P.; Grey, C. P., In situ NMR and electrochemical quartz crystal microbalance techniques reveal the structure of the electrical double layer in supercapacitors. *Nature Materials* **2015,** *14* (8), 812-819.
12. Thompson, W. H., Perspective: Dynamics of confined liquids. *The Journal of Chemical Physics* **2018,** *149* (17), 170901.
13. Bonthuis, D. J.; Gekle, S.; Netz, R. R., Dielectric profile of interfacial water and its effect on double-layer capacitance. *Physical Review Letters* **2011,** *107* (16), 166102-166102.
14. Bonthuis, D. J.; Netz, R. R., Unraveling the combined effects of dielectric and viscosity profiles on surface capacitance, electro-osmotic mobility, and electric surface conductivity. *Langmuir* **2012,** *28* (46), 16049-16059.
15. Kong, X.; Jiang, J.; Lu, D.; Liu, Z.; Wu, J., Molecular theory for electrokinetic transport in pH-regulated nanochannels. *Journal of Physical Chemistry Letters* **2014,** *5* (17), 3015-3020.
16. Kondrat, S.; Wu, P.; Qiao, R.; Kornyshev, A. A., Accelerating charging dynamics in subnanometre pores. *Nature Materials* **2014,** *13* (4), 387-393.
17. Lee, A. A.; Kondrat, S.; Oshanin, G.; Kornyshev, A. A., Charging dynamics of supercapacitors with narrow cylindrical nanopores. *Nanotechnology* **2014,** *25* (31), 315401.
18. Hoffmann, J.; Gillespie, D., Ion correlations in nanofluidic channels: effects of ion size, valence, and concentration on voltage- and pressure-driven currents. *Langmuir* **2013,** *29* (4), 1303-1317.

19. Lian, C.; Zhao, S.; Liu, H.; Wu, J., Time-dependent density functional theory for the charging kinetics of electric double layer containing room-temperature ionic liquids. *The Journal of Chemical Physics* **2016,** *145* (20), 204707.
20. Xin, Y.; Zheng, Y. X.; Yu, Y. X., Density functional theory study on ion adsorption and electroosmotic flow in a membrane with charged cylindrical pores. *Molecular Physics* **2016,** *114* (16-17), 2328-2336.
21. Wu, P.; Qiao, R., Physical origins of apparently enhanced viscosity of interfacial fluids in electrokinetic transport. *Physics of Fluids* **2011,** *23* (7), 072005.
22. Gillespie, D., High energy conversion eficiency in nanofluidic channels. *Nano Letters* **2012,** *12* (3), 1410-1416.
23. Feng, G.; Qiao, R.; Huang, J.; Sumpter, B. G.; Meunier, V., Ion distribution in electrified micropores and its role in the anomalous enhancement of capacitance. *ACS Nano* **2010,** *4* (4), 2382-2390.
24. Qiu, Y.; Chen, Y., Capacitance performance of sub-2 nm graphene nanochannels in aqueous electrolyte. *The Journal of Physical Chemistry C* **2015,** *119* (42), 23813-23819.
25. Su, J.; Huang, D., Coupling transport of water and ions through a carbon nanotube: the role of ionic condition. *The Journal of Physical Chemistry C* **2016,** *120* (20), 11245-11252.
26. Lagadec, M. F.; Zahn, R.; Muller, S.; Wood, V., Topological and network analysis of lithium ion battery components: the importance of pore space connectivity for cell operation. *Energy & Environmental Science* **2018,** *11* (11), 3194-3200.
27. Lian, C.; Su, H.; Li, C.; Liu, H.; Wu, J., Non-negligible roles of pore size distribution on electroosmotic flow in nanoporous materials. *ACS Nano* **2019,** *13* (7), 8185-8192.
28. Gao, J.; Liu, X. L.; Jiang, Y. N.; Ding, L. P.; Jiang, L.; Guo, W., Understanding the giant gap between single-pore- and membrane-based nanofluidic osmotic power generators. *Small* **2019,** *15* (11), 1804279.
29. Cheng, C.; Jiang, G.; Garvey, C. J.; Wang, Y.; Simon, G. P.; Liu, J. Z.; Li, D., Ion transport in complex layered graphene-based membranes with tuneable interlayer spacing. *Science Advances* **2016,** *2* (2), e1501272.
30. Hess, B.; Kutzner, C.; van der Spoel, D.; Lindahl, E., GROMACS 4: Algorithms for highly efficient, load-balanced, and scalable molecular simulation. *Journal of Chemical Theory and Computation* **2008,** *4* (3), 435-447.
31. Berendsen, H. J. C.; Grigera, J. R.; Straatsma, T. P., The missing term in effective pair potentials. *The Journal of Physical Chemistry* **1987,** *91* (24), 6269-6271.
32. Chatterjee, S.; Debenedetti, P. G.; Stillinger, F. H.; Lynden-Bell, R. M., A computational investigation of thermodynamics, structure, dynamics and solvation behavior in modified water models. *The Journal of Chemical Physics* **2008,** *128* (12), 124511.
33. Vanommeslaeghe, K.; Hatcher, E.; Acharya, C.; Kundu, S.; Zhong, S.; Shim, J.; Darian, E.; Guvench, O.; Lopes, P.; Vorobyov, I.; Mackerell Jr, A. D., CHARMM general force field: A force field for drug-like molecules compatible with the CHARMM all-atom additive biological force fields. *Journal of Computational Chemistry* **2010,** *31* (4), 671-690.
34. Bjelkmar, P.; Larsson, P.; Cuendet, M. A.; Hess, B.; Lindahl, E., Implementation of the CHARMM force field in GROMACS: analysis of protein stability effects from correction maps, virtual interaction sites, and water models. *Journal of Chemical Theory and Computation* **2010,** *6* (2), 459-466.
35. Prajapati, J. D.; Mele, C.; Aksoyoglu, M. A.; Winterhalter, M.; Kleinekathöfer, U., Computational modeling of ion transport in bulk and through a nanopore using the drude polarizable force field. *Journal of Chemical Information and Modeling* **2020,** *60* (6), 3188-3203.

36. Essmann, U.; Perera, L.; Berkowitz, M. L.; Darden, T.; Lee, H.; Pedersen, L. G., A smooth particle mesh Ewald method. *The Journal of Chemical Physics* **1995,** *103* (19), 8577-8593.
37. Kirkpatrick; Scott, Classical transport in disordered media: scaling and effective-medium theories. *Physical Review Letters* **1971,** *27* (25), 1722-1725.
38. Burganos, V. N.; Sotirchos, S. V., Diffusion in pore networks: Effective medium theory and smooth field approximation. *AIChE Journal* **1987,** *33*, 1678-1689.
39. Bukowski, B. C.; Keil, F. J.; Ravikovitch, P. I.; Sastre, G.; Snurr, R. Q.; Coppens, M.-O., Connecting theory and simulation with experiment for the study of diffusion in nanoporous solids. *Adsorption* **2021,** *27* (5), 683-760.
40. Jiang, D.-e.; Jin, Z.; Wu, J., Oscillation of capacitance inside nanopores. *Nano Letters* **2011,** *11* (12), 5373-5377.
41. Lian, C.; Gallegos, A.; Liu, H.; Wu, J., Non-scaling behavior of electroosmotic flow in voltage-gated nanopores. *Physical Chemistry Chemical Physics* **2016,** *19* (1), 450-457.
42. Tao, H.; Lian, C.; Liu, H., Multiscale modeling of electrolytes in porous electrode: From equilibrium structure to non-equilibrium transport. *Green Energy & Environment* **2020,** *5* (3), 303-321.